



HAL
open science

Effects of heat transfer coefficient variations on composite curing

Adam Fisher, Arthur Lévy, James Kratz

► **To cite this version:**

Adam Fisher, Arthur Lévy, James Kratz. Effects of heat transfer coefficient variations on composite curing. *Journal of Composite Materials*, 2022, pp.002199832211455. 10.1177/00219983221145506 . hal-03919725

HAL Id: hal-03919725

<https://hal.science/hal-03919725>

Submitted on 3 Jan 2023

HAL is a multi-disciplinary open access archive for the deposit and dissemination of scientific research documents, whether they are published or not. The documents may come from teaching and research institutions in France or abroad, or from public or private research centers.

L'archive ouverte pluridisciplinaire **HAL**, est destinée au dépôt et à la diffusion de documents scientifiques de niveau recherche, publiés ou non, émanant des établissements d'enseignement et de recherche français ou étrangers, des laboratoires publics ou privés.

Effects of heat transfer coefficient variations on composite curing

Adam Fisher^{a,b}, Arthur Levy^b, James Kratz^{a,*}

^aBristol Composites Institute, University of Bristol, Queen's Building, University Walk, Bristol BS8 1TR, United Kingdom

^bNantes Université, CNRS, Laboratoire de thermique et énergie de Nantes, LTeN, UMR 6607, F-44000 Nantes, France

Email address: james.kratz@bristol.ac.uk

Abstract

Composite laminates are classically manufactured by curing in a vessel. The environment inside the processing vessel dictates the efficiency and ultimately drives the quality of thermoset composite parts.

Experimental measurements of spatial heat transfer coefficients were conducted on industrial scale vessels, including autoclaves and large ovens. The final part quality was investigated using the experimental data as input to a coupled heat transfer and curing model.

Measurements showed that heat transfer coefficients in autoclaves were greater in magnitude and spatial variability. The distribution in the autoclaves followed a pattern common in the literature, in contrast to that in the ovens which varied considerably between devices.

Numerical predictions indicated autoclave measured heat transfer coefficients provide less lag to the imposed temperature history and smaller temperature overshoots. However, the greater robustness to variability at autoclave heat transfer coefficients was offset by the greater variability, resulting in comparable robustness across the ovens and autoclaves.

Keywords: Heat transfer coefficient, curing, variability, autoclave, oven, thermoset laminate.

1. Introduction

The central element in processing thermoset laminates is the application of heat, this triggers the curing reaction through which desirable properties are acquired. Historically, aerospace grade thermoset laminates have been processed in autoclaves, where the ability to apply a compaction pressure in addition to temperature provides superior consolidation in the final part¹. More recently, the desire to produce larger parts with less energy and cost has motivated the use of Out-Of-Autoclave manufacturing². This work focuses on vacuum bag only oven consolidation, where the available compaction pressure is limited to 1 atmosphere. As will be discussed, the inability to apply higher pressure can have negative consequences beyond just poor consolidation.

Material manufacturers often provide a recommended set of processing conditions for a material, this will include a temperature and a pressure cycle (the latter if an autoclave is recommended). However, having the processing environment in-line with these recommendations is not sufficient for producing quality parts. In autoclaves and ovens, forced convection is typically the main source of heat transfer into a part, therefore, it also largely controls the rate of chemical and physical transformation during cure³. Measurements

by Kluge et al⁴ showed significant temperature differences across a tool in an autoclave, demonstrating the consequences of HTC variation. Through analysing large quantities of defect data Wang et al⁵ found the failure to achieve a homogeneous cure within a part can induce voids, resin rich regions, pores and delamination, and excessive temperature overshoots have also been observed⁶.

The effectiveness of convective heat transfer from the vessel gas to the part is classically modelled using the convective heat transfer coefficient h_{con} (HTC). HTC is defined as;

$$h_{con} = \frac{q}{T_s - T_\infty} \quad (1)$$

where q is the heat flux across the boundary in $\text{Wm}^{-2}\text{K}^{-1}$, T_s is the surface temperature and T_∞ is the surrounding gas temperature.

Given the importance of convective heat transfer, studies have been conducted to understand how the value of HTC can vary within an autoclave, Ghamlouch³ presented a comprehensive overview. This analysis routinely involves lumped mass calorimeters. The use of plate calorimeters is common, these are typically insulated at the edges to allow the assumption of 1-dimensional (1D) heat transfer, the validity of these assumptions was demonstrated by Bohne et al⁷ using Finite Elements (FE). Measurements are taken using thermocouples at locations along the length of the plate. Slesinger et al⁶ demonstrated that calorimeters consisting of a cylindrical metal rod could produce similar results to a plate, which is advantageous due to the much smaller size. It was through measurements made in this fashion that the connection was demonstrated between the local velocity field and the value of HTC^{3, 8}, the typical lack of uniformity in autoclave gas flow fields⁶ explaining the large amounts of observed variability.

A number of studies have focused on providing detailed analysis of the thermal environment within autoclaves^{4, 6, 9-11}. Studies mapping the distribution of HTC within an autoclave consistently found large spatial variations. For example, Slesinger et al⁶ found a variation from 60 to 200 $\text{Wm}^{-2}\text{K}^{-1}$ in a 1.5m long autoclave with a 1.15m diameter and Bohne et al⁷ found a variation from 70 to 110 $\text{Wm}^{-2}\text{K}^{-1}$ in a 2m long autoclave with a 1m diameter. In the study by Kluge et al⁴, it was noted spatial HTC values appear to depend on the configuration of the autoclave, increasing pressure or flow velocity augments them while maintaining the existing pattern.

Autoclave layouts generally vary little from that shown in Figure 1, as such there has been an agreement between the HTC distributions reported by different studies, higher values are found at the front and decrease towards the back as the high velocity inlet air recirculates off the door and flows to the recirculating fan at the back of the vessel^{3, 12}. This deduced flow pattern has been confirmed using CFD analysis⁶. Johnston¹³ demonstrated the need to consider multiple devices to deduce general relationships, when one of the three autoclaves considered showed a contradictory decrease in HTC at higher pressures, this was attributed to insufficient fan power to accommodate the resulting air density increase.

Despite the increasing use of ovens for processing composites, there appears to be no analysis of the HTC distribution within ovens analogous to the autoclave examples given above. This is surprising given the lack of applied pressure causes variability in the processing environment to have more influence on the properties of the final part. This was

demonstrated by Kluge et al⁴, when applying the same temperature history with and without applied pressure it was found that the application of pressure significantly reduced the front-back temperature difference in the tool. The greater sensitivity of HTC to pressure compared to the temperature history in autoclaves has been widely reported^{7, 13}.

Motivated by this absence in the literature, the first part of this study includes the analysis of HTC in ovens. The work presented shows the dependence of HTC on internal geometry and the gas circulatory system³. To verify this for ovens, a range of oven sizes is considered, and particular attention is given to the influence of features such as shape, size, inlet, and exhaust locations. For comparison, the HTC distributions inside two autoclaves are also considered. Mapping the devices under the same conditions enables any common trends and differences to be identified, allowing a distinction to be made between what can be assumed to be generally applicable and what must be considered on a case-by-case basis.

The resulting properties of a part manufactured in such a vessel are linked to the mechanics during the curing process¹⁴. At gelation, the degree of cure (DOC) the resin transitions between a viscous and a rubbery state, there are significant changes in material properties, including shrinkage and the ability to sustain stresses¹⁵. For a given resin system chemistry, the time for gelation to occur depends on temperature history¹⁶, hence temperature gradients can lead to non-uniformities through the material^{17, 18}. Thus, to fully understand the effect of heat transfer variability on the final part, cure kinetics must be considered. Given the cure kinetics are driven by heat transfer in the material, a coupled approach, first proposed by Loos and Springer¹⁹, is required to predict the phenomena.

To understand the consequence of HTC nonuniformity on the curing reaction, in the second part of this study, an FE model will be used to solve coupled heat transfer and cure kinetics equations. Laminate thickness is typically much smaller than the in-plane dimensions, enabling an efficient 1D modelling through thickness. Five indicators shall be considered to capture the influence of HTC variability on the curing process, two refer to the transverse temperature distribution in isolation, the other three take cure kinetics into account.

In consideration of heat transfer, the lag between the imposed conditions and those in the laminate, and the uniformity of conditions within the laminate shall be studied. In consideration of cure kinetics, processing efficiency, the likelihood of residual stresses, and excessive temperature will be the focus. Measured HTC data from the different vessels is used in the FE model to investigate the distinctions between curing in an oven and an autoclave.

2. Experimental Mapping of HTC in Ovens and Autoclaves

2.1 Methods

2.1.1 Temperature measurements

Calorimeter measurements were taken in seven vessels: five ovens and two autoclaves. Descriptions of each vessel and the measurement conditions are provided in Table 1. Figure 1 shows examples of how measurements were taken in the ovens and autoclaves, the images demonstrate the arrays of calorimeters used to take temperature measurements at fixed sets of locations within the volumes of each vessel, apart from which they were empty. Note that although this indicated the expected level of variability within the vessels, in practice the

moulds and parts will have a strong influence on the flow conditions¹³, which is not captured here.

2.1.2 Heat transfer coefficient estimation

The calorimeters, assumed to be lumped masses, consisted of two K-type thermocouples, one inside a stainless-steel 304 rod of length 0.1m and diameter 0.025m, the other on the outside to measure the local air temperature. The temperature measurements from the two thermocouples enabled a global calorimeter HTC to be estimated through the following procedure.

Total heat \dot{Q} input in the calorimeter can be determined for a given temperature increase \dot{T}_c as

$$\dot{Q} = \iiint \rho_c C_{p_c} \dot{T}_c dV \quad (2)$$

where ρ_c is the density, C_{p_c} is the specific heat capacity and T_c is temperature of the calorimeter. Temperature was considered uniform in the calorimeters, the integral became equivalent to

$$\dot{Q} = \rho_c V C_{p_c} \dot{T}_s \quad (3)$$

where V is the calorimeter volume and for convention, T_s is the calorimeter surface temperature. Substituting this simplified form into Equation (1) yielded the expression that was used to compute the HTC from the experimental data

$$h_{con} = \frac{\rho_c V C_{p_c} \dot{T}_s}{A_s (T_s - T_\infty)} \quad (4)$$

where A_s is the calorimeter surface area. The temperature data (T_s, T_∞) used to calculate the HTC was limited to that of the thermocouples during the ramp up. During this sliding regime, $T_s - T_\infty$ was approximately constant for all calorimeters, with the standard deviations typically around 2°C. The reported value of HTC for each set of calorimeter measurements was the mean of all the values computed during this period. Assuming noise to be random, this approach helped to reduce the influence of the noise from the thermocouple measurements. In the case of oven 5, the measurements from the first ramp (Table 1) were used due to the superior quality of the recorded data.

2.1.3 Validating the lumped mass assumption

Biot number is defined as

$$Bi = \frac{h_{con} l}{k} \quad (5)$$

where h_{con} is HTC, l and k are the characteristic length and thermal conductivity of the object. The characteristic length can be taken as the ratio of volume to surface area, for a cylinder this is equal to half the radius. The horizontal surfaces of the cylinders were partially obscured, to be conservative, they were not accounted for. The cylinders had radii of 0.0125m and thermal conductivities of 14 Wm⁻¹K⁻¹, this gave a Biot number of roughly 0.00045 h_{con} . For Biot numbers below 0.1 a uniform temperature assumption is valid²⁰. This gave a maximum allowable HTC of 224Wm⁻²K⁻¹. Given the greatest measured HTCs of 203Wm⁻²K⁻¹ and

62Wm⁻²K⁻¹ in the autoclaves and ovens respectively, the assumption was valid in both vessels.

2.1.4 Checking for negligible radiative heat transfer

Radiative heat transfer is computed according to the Stefan-Boltzmann law of radiation

$$q_{rad} = \varepsilon\sigma(T_{wall}^4 - T_{cal}^4) \quad (6)$$

where q_{rad} is the heat flux into the calorimeter, ε is the calorimeter emissivity, T_{cal} and T_{wall} are the temperatures of the calorimeter and wall respectively, and σ is the Stefan-Boltzmann constant. When the mean (T_m) of T_{cal} and T_{wall} is much greater than the difference between them (ΔT) (i.e. $(\Delta T/T_m)^2/4 \ll 1$), which is the case here, Equation (6) can be linearised into the same form as Equation (1)²¹. As the calorimeters are much smaller than the vessels, the view factor can be omitted and the resulting coefficient of radiative heat transfer writes

$$h_{rad} = 4\sigma T_m^3 \varepsilon \quad (7)$$

The calorimeters were stainless steel 304 which has emissivity between 0.32-0.38^{22, 23}. To be conservative, the upper bound, $\varepsilon = 0.38$, was assumed.

To be conservative, T_{wall} was assumed equal to the air temperature. The ratio of h_{con} to h_{rad} was between 3 and 15 in the ovens and between 160 to 650 in the autoclaves. In line with the literature for similar ratios²⁴, it was deemed acceptable to assume h_{con} was the sole contribution to HTC (h) in both sets of vessels.

2.2 Experimental Results

2.2.1 HTC variability between the vessels

The temperature and pressure dependence of HTC in turbulent flow is¹³:

$$h \propto \left(\frac{p}{T}\right)^{\frac{4}{5}} \quad (8)$$

This indicates the results from oven 5 are not directly comparable to the others due to the different temperature history used, they are included as a further example. Conversely, literature^{7, 13} suggests when the relative change in pressure is much greater than temperature, as in the autoclave cycles, HTC can be approximated solely as a linear function of pressure, the dependence on temperature and heating rate being minor.

The measured HTC values in addition to data from Slesinger⁶ are summarised in Figure 2, the plotted values are the means, and the error bars represent the standard deviations taken over the calorimeters in each vessel. The error bars at 1 and 7 bars represent the standard deviation of HTC for all the vessels at these pressures to aid visualisation. The pressure dependence of HTC described in Equation (8) is shown to follow the general trend of the measurements. A fitting coefficient of 29.3 was found to minimise the mean squared error between Equation (8) and the measurements.

The results showed little difference between the mean HTC in each trial for all vessels. This result reflects the conclusions from autoclave measurements in the literature which showed little change under constant pressure⁷. Run-to-run variability is lowest in the ovens followed by the autoclaves at 3 and 3.5 bars. In all autoclaves the run-to-run difference increased at 7

bars. This trend can be interpreted using the link between the gas flow and HTC. Air density increases with pressure, Reynolds number is proportional to density, therefore, the less repeatable HTC distributions at elevated pressure result from greater turbulence in the gas flow.

The effect of applied pressure is clear when the mean HTC values from the ovens are compared with those from the autoclaves. The autoclaves have greater values in all cases, particularly when operated at 7 bars. This trend is to be expected given Equation (8), however the results suggest this relationship has a tendency to overpredict the influence of pressure. When scaled accordingly, the HTC predicted for the oven data consistently exceeded the values measured in the autoclaves, indicating the presence of other influential factors, for example the more significant radiative contribution to the oven measured HTC. The greater HTC in the large ovens is likely due to more powerful gas circulatory systems providing higher air speeds.

2.2.2 Spatial HTC variability within the vessels

The standard deviations displayed in Figure 2 represent the spatial variability in HTC during the two trials. Interestingly, in the oven data, there is no clear relationship between size and the level of spatial variability, the second smallest oven produced the lowest standard deviation, yet the largest oven displayed a lower value than the smallest oven. The absence of a standard configuration among ovens likely contributed to the lack of consistency. The large value for Oven 5 was due to a single extreme measurement, which was attributed to the proximity of the calorimeter to the exhaust, discounting this gives the more reasonable standard deviation of $4.1 \text{ Wm}^{-2}\text{K}^{-1}$. Among the three autoclaves in Figure 2, there is a trend towards decreasing spatial variability with increasing size.

There is a noticeable difference between the observed spatial variability in the ovens compared to the autoclaves. This difference can likely be attributed to the techniques used to achieve high HTC in the autoclaves. In addition to elevated pressure, HTC and Reynolds number are positively correlated with air velocity, motivating high inlet air speeds. Due to the way air flows are generally setup in autoclaves³ this causes a big contrast in the airspeed at the front to that at the back, producing the high spatial variability in HTC.

To provide a summary of the spatial HTC variability within the ovens and autoclaves more generally, Figure 3 presents a boxplot of the measurement grouped by vessel type. The autoclave measurements at the different pressures are treated separately due to the strong influence of pressure on HTC. The large range of values measured in the autoclaves is consistent with the literature^{6,7}. The largest HTC values occurred around the front and the smallest at the back in accordance with the air flow pattern discussed above. When comparing the oven results with the autoclave results, and the 3 bars autoclave with the 7 bars autoclave results, an apparent trend emerges with greater pressure resulting in a broader range of measured values. Despite this, in the autoclaves, the spatial variability represented by the inter-quartile range appears to be unaffected by the change in pressure, this latter result supports the literature^{4,13} which reported the preservation of patterns in the HTC field with changes in pressure.

The spatial disparities observed in the ovens were generally smaller. The uniquely large maximum HTC of $105 \text{ Wm}^{-2}\text{K}^{-1}$ in oven 5 (the second largest was $51 \text{ Wm}^{-2}\text{K}^{-1}$) was the cause

of the large variability presented in Figure 2. The smaller inter-quartile range of the oven data reflects the low spatial variability measured in the ovens. The skew of the oven data towards higher values is due to the lower values ($<24\text{Wm}^{-2}\text{K}^{-1}$) being solely contributed by oven 3, the size of these measurements was attributed to the shelves which would have obstructed the airflow, lowering the velocity. Lacking a standard configuration like the autoclaves, the recorded HTC field patterns varied among the ovens, in practice this necessitates a case-by-case approach to analysis of oven environments.

3. Numerical Methods and Results

3.1 Numerical Modelling

Coupled cure kinetics and transient heat transfer equations were solved using the FE method to capture the curing process through the thickness of a carbon fibre reinforced thermoset laminate.

3.1.1 Numerical implementation

The curing process of the thermoset laminate was modelled using FE in COMSOL Multiphysics to solve coupled heat transfer and cure kinetics equations. The cure kinetics model was derived by Mesogitis et al²⁵ by fitting differential scanning calorimeter data to an adapted version of the Kamal and Sourour model²⁶ and was validated against experimental data.

It was assumed that the in-plane dimensions of the laminate far exceeded the thickness, hence the in-plane temperature gradients could be treated as negligible, allowing a 1D approximation of heat transfer²⁷. Furthermore, spatial variability in HTC will have a negligible effect on the in-plane temperature gradient compared to the transverse gradient.

The geometry of the 1D model is represented in Figure 4, it consisted of a homogenised thermoset composite laminate in ideal contact with a 10mm thick invar tool. The origin was taken to be at the interface between the two domains, this approach facilitated independent analysis of the two domains.

The properties of the homogenised laminate were representative of Hexply M21 carbon fibre epoxy prepreg^{25, 28}. Simulations were performed with part thicknesses of 5mm, 10mm and 15mm. These specific geometries were considered for illustrative purposes. It is noted that although the trends will be applicable, any such example will lack generality due to the strong influence of geometric parameters such as the laminate and tool thicknesses on the curing process⁶.

The heat transfer component of the model was implemented using the 'Heat Transfer in Solids' physics in COMSOL. The heat equation is a first order in time and second order in space partial differential equation, therefore requires an initial condition and two boundary conditions to solve. The initial condition was that the system started at a temperature of 20°C. The boundary conditions were convective, applied to the two ends of the geometry. The air temperature history followed by T_{∞} during this study was based on the recommended cycle for Hexply M21²⁸. It consisted of a 2°C per minute ramp from 20°C followed by a dwell at 180°C for 2 hours, which is a typical curing cycle for aerospace grade epoxy systems.

The cure kinetics model was implemented in COMSOL as a distributed ordinary differential equation applied to the laminate domain. Computations were performed assuming an initial degree of cure of 0.01 to escape the singular stationary point of the model.

The implementation of the coupled model into COMSOL was validated through a comparison with experimental data²⁵.

3.1.2 Dimensional analysis

As detailed in the appendix, the dimensionless forms of the heat equations applied to the laminate and tool domains respectively were

$$\frac{dT^*}{dt^*} = Fo_c \frac{d^2T^*}{dx^{*2}} + P_h \frac{d\alpha}{dt^*} \quad (9)$$

$$\frac{dT^*}{dt^*} = Fo_t \frac{1}{A^2} \frac{d^2T^*}{dx^{*2}} \quad (10)$$

where Fo_c and Fo_t are the composite and tool Fourier numbers respectively, A is the laminate to tool thickness ratio and P_h is the phase transition number.

The convective boundary conditions applied to the free edge of the laminate and tool domains became

$$\left. \frac{dT^*}{dx^*} \right|_{x^*=1} = -Bi_c [T^*(t) - T_\infty^*(t)] \quad (11)$$

$$\left. \frac{dT^*}{dx^*} \right|_{x^*=-\frac{1}{A}} = -Bi_t A [T^*(t) - T_\infty^*(t)] \quad (12)$$

where Bi_c and Bi_t are the composite and tool Biot numbers respectively.

The dimensionless cure kinetics equation is given as

$$\frac{d\alpha}{dt^*} = t_c [k_1(1 - \alpha)^{n_1} + k_2\alpha^m(1 - \alpha)^{n_2}] \quad (13)$$

3.1.3 Parametric study

To explore the effect of the observed spatial variability in HTC on the temperature distribution through the thickness of the laminate, FE simulations were performed. Two metrics were used,

- i. The time to reach steady state at the imposed dwell temperature through the thickness. A 1°C margin above was added for robustness
- ii. The absolute difference between the temperature of the hottest and coldest nodes at each time

These metrics capture the lag between the prescribed temperature and those in the laminate, and temperature inhomogeneity in the laminate itself. HTCs representing low and high oven values, and an autoclave at 7 bars were considered (Table 2).

Further simulations were performed to investigate how the curing process of an epoxy composite laminate was affected by HTC. For completeness the HTC range from Figure 3

was considered, it is noted the extreme values are outliers. While these values reflect the environment within the devices, it is important to note the absence of a vacuum bag which reduces the HTC seen by manufactured parts.

The influence of HTC on the curing process was characterised using three metrics:

- i. Cure time, the time for the DOC to exceed 90% through the thickness
- ii. Temperature overshoot, the greatest positive difference between the predicted temperature and the 180°C dwell temperature through the thickness
- iii. Gel time, the time for the DOC to reach gelation (assumed to be 50% DOC) through the thickness

The simulations were performed with the parameters listed in Table 2.

3.2 Numerical Results

3.2.1 Dimensional analysis

The Biot number in the nondimensionalised boundary conditions indicated the need to model the temperature gradient through the domains. Figure 5 shows Biot number was lowest at the smallest values of HTC and thickness. The value for the laminate never dropped below the 0.1 threshold required to assume lumped capacitance, justifying the need to model the heat transfer within it. The middle plot in Figure 5 shows lumped capacitance could only be assumed in the tool for HTCs less than $150\text{Wm}^{-2}\text{K}^{-1}$, hence for consistency across the analyses, the temperature field in the tool was fully computed in all simulations.

Fourier number gives the ratio of the rate of heat transfer to the rate of heat storage. Fourier number is greater with a thinner part, indicating efficient dissipation of exothermic heat, combating the occurrence of severe temperature overshoots. Owing to the much greater conductivity of invar, the tool Fourier number of 176 far exceeded any of the laminate values shown in Figure 5. The ability of the tool to transfer heat much faster than accumulating it makes it influential in dispersing exothermic heat. Being significantly greater than unity, the Fourier numbers indicate the need to model conduction $\left(\frac{d^2T}{dx^2}\right)$ in both domains.

Phase transition number gives the ratio of the exothermic heat to the amount of heat available due to the temperature ramp. Values greater than unity indicate the curing reaction is the dominant form of heating during the ramp, suggesting the occurrence of a highly influential exotherm. In this case, Ph was 0.86, below unity, indicating the environment was the primary source of heating, however, its proximity to one indicates the relevance of the exotherm and justified the coupling of the two sub-models.

3.2.2 Effect of HTC on through thickness temperature

3.2.2.1 Time to reach the prescribed dwell temperature

Figure 6 illustrates the effect of HTC on the temperature history in a 10mm thick laminate. With this thickness, the effect of position in the laminate is negligible compared to the effect of the changes in HTC. The difference between the three sets of curves reflects the non-linearity in Figure 7, a bigger change occurring with the step from $25\text{Wm}^{-2}\text{K}^{-1}$ to $50\text{Wm}^{-2}\text{K}^{-1}$ despite its smaller size. The reduced time with increasing HTC shown in Figure 7 is clearly attributed to the smaller temperature lag with the surroundings during the ramp and the smaller temperature overshoot.

3.2.2.2 Establishing through thickness temperature homogeneity

Figure 8 shows how the maximum transverse temperature difference changes with time in a 10mm part. Analogous trends were observed for the other part thicknesses, with values that were scaled in proportion to the thickness, according to the change in Biot number.

The trends in Figure 8 are reflective of a higher HTC helping to impose the ramp up and mitigate overheating due to the exotherm. The key points can be explained by considering the heat transfer from the two sources of heat, the environment, and the exothermic curing reaction.

The initial heat input is solely from the environment via convective heat transfer, so the air/laminate boundary is initially the hottest point of the laminate, and the centre the coolest. The increasing temperature difference is due to the low transverse conductivity. The temperature difference peaks at the end of the ramp, beyond this point convective heating from the environment becomes less significant.

The minima represent the points at which the location of highest temperature moves from the boundary into the laminate because of the exotherm. The second maxima represent the peak temperature overshoots, the centre of the laminate is hottest and the boundary the coldest.

3.2.3 Effect of HTC on cure through the thickness

3.2.3.1 Cure time

Cure time as defined in Section 3.1.5 varied in a non-monotonic fashion as HTC increased. Figure 9 illustrates this relationship for the three part thicknesses considered. Initially cure time decreased with increasing HTC, taking a minimum value between 25 and 35 $\text{Wm}^{-2}\text{K}^{-1}$, before increasing.

This relationship can be expressed by considering Figure 6. At HTCs below the minima the resistance at the boundary is too great for effective heating. At HTCs above the minima the low resistance at the boundary reduces the influence of exothermic heat. The minima represent a balance of the two effects; however, it is unlikely to be optimal due to overheating.

The error bars represent 95% confidence intervals for the HTCs measured in three types of vessels, assuming normal distributions. To maximise generality, measurements from the ovens and autoclaves were grouped together, as in Figure 3. They illustrate the range of cure times possible with a 10mm thick part.

The lower minimum with increasing part thickness can be attributed to greater temperature overshoot (Figure 10). The offsets are due to the higher Biot numbers indicated in Figure 5.

Cure time depends on the node where cure occurs slowest. As Biot number increases the exothermic heating at the centre has less influence on the boundary. Hence the convergence of cure times beyond the minima.

3.2.3.2 Temperature overshoot

The curves in Figure 10 are highly similar, the thickness increases mostly causing a translation. The size of the translation is clearly non-linear, the increasing difference reflecting the change in Fourier number and the Arrhenius temperature dependence of the cure kinetics²⁵. The same 95% confidence interval error bars as in Figure 9 have been applied to mark the possible overshoot variation in a 10mm thick part.

As Biot number increases the temperature distribution through the thickness becomes less uniform, the resulting temperature gradient combined with the lower boundary resistance increases the dispersion of exothermic heat in accordance with Fourier and Darboux²⁹.

3.2.3.3 Gel time

Gel time as defined in Section 3.1.5 decreases with increasing HTC as shown in Figure 11. As with cure time, at high values of HTC, the gel times for the different thicknesses converge. Again, this is attributed to the increasing dominance of conductive resistance making the reaction at the boundary increasingly dependent on the environment and less dependent on the exothermal heating centred at the middle of the part.

Unlike cure time, gel time decreases monotonically with increasing HTC. The difference is made clear by Figure 6, for the HTCs measured, the gel time (when DOC reaches 0.5) elapsed before the temperature overshoot (occurring at DOC of around 0.8). Therefore, the change in gel time due to HTC is only affected by the effective ramp rate in the material which increases with HTC, and not exotherm effects.

4 Discussion

4.1 Efficiency-Quality Trade-Off

For this combination of configuration and temperature history, none of the ovens have sufficient HTCs ($>45\text{Wm}^{-2}\text{K}^{-1}$) throughout to prevent temperature overshoots exceeding 10°C for any of the part thicknesses studied here. With the non-linear increase of temperature overshoot with part thickness noted in Section 3.2.3.2, although the 5mm part can be safely cured in the autoclaves, only autoclave 1 at 7 bars is suitable for the 15mm part. This level of overshoot is significant for M21 as phase changes have been reported above these temperatures²⁵.

The flattening of the temperature overshoot-HTC curve in Figure 10 highlights the limitations of the curing environment for reducing temperature overshoot. The cure cycle used is representative of one typically used with thinner parts, a relatively high ramp rate (2°Cmin^{-1}) with no pre-dwell. It is clearly not suitable for curing M21 composite parts in oven environments. To reduce the rate of exothermic heating, features such as pre-dwells and slower temperature ramps must be added. However, these features can significantly reduce processing efficiency, hence by operating in autoclave HTC regimes, greater part thicknesses can be processed before such inefficiencies are necessary.

4.2 Effect of Spatial Heat Transfer Coefficient Variability

The error bars in Figures 9 and 10 were used to consider how the spatial variability in HTC could propagate through the curing process, using cure time and temperature overshoot for a 10mm thick part as metrics. The ranges of cure time and temperature overshoot corresponding to the bounds of the error bars for the three types of vessels are shown in Table 3.

With a mean HTC of $37\text{Wm}^{-2}\text{K}^{-1}$ the oven confidence interval straddles a steep section of the cure time-HTC curve (Figure 9). Despite this, the small spatial variability of HTC in the ovens resulted in a narrow range of cure time values. In contrast, the respective means of $99\text{Wm}^{-2}\text{K}^{-1}$ and $138\text{Wm}^{-2}\text{K}^{-1}$ for the autoclaves at 3 and 7 bars were on much shallower sections of the curve. However, due to the greater spatial variability in these vessels, this advantage from the higher HTCs was largely offset. Consequently, the range of cure times predicted for the three types of vessels were similar, the closest ranges being for the ovens and autoclaves at 3 bars, with the autoclaves at 7 bars having the narrowest range. These results show the much greater robustness to HTC variability at higher HTC values.

The more comparable gradients at oven and autoclave HTCs in Figure 10 meant the lower spatial variability in the ovens produced a range of cure times practically indistinguishable from the autoclaves. The oven range was narrower than predicted for the autoclaves at 3 bars and essentially the same as the autoclaves at 7 bars. Hence, for practical purposes, the predictability of overshoot is consistent among the vessels.

In terms of the overshoot values themselves, even the lower bound of the oven was excessive. Whereas both autoclaves had upper bounds below the 10°C threshold imposed by the material. This suggests only the autoclaves were capable of curing the 10mm thick part reliably.

The monotonic nature of Figure 10 results in a simpler interpretation for temperature overshoot, where higher HTC values result in a lower mean and greater robustness to HTC variability. Furthermore, the rate of improvement diminishes at a slower rate as HTC increases compared to cure time.

5 Conclusion

The curing of composite laminates on a mould, in a vessel (oven or autoclave) is driven by heat transfer. Classically, heat transfer within the part is modelled using a convective heat transfer coefficient (HTC) at the boundaries.

In this study, experimental HTC data from a range of oven sizes, including two large pre-production ovens, was compared to autoclave data. Statistical analysis was conducted to investigate the spatial variability of HTC within the vessels. A coupled Finite Element model was used to propagate the measured uncertainty through the curing reaction to predict the effects on final part quality. The effects were assessed using five indicators, two to consider temperature and three for the cure reaction.

The temperature indicators showed that the temperature history was more successfully imposed with the higher HTCs measured in the autoclaves. This is realised with less temperature lag during the ramp-up and smaller temperature overshoot during exothermic reaction.

The key result was that despite the greater robustness to spatial HTC variability at autoclave HTCs, the larger variability in the autoclave HTC data resulted in similar robustness of the cure reaction indicators across all vessel types.

This study considered a single cure cycle, one recommended for laminate thicknesses of less than 15mm^{28} . Future work could consider the effect of using different cure cycles, for

example with different ramp rates and a pre-dwell. These cure cycle parameters could then be optimised for a given combination of vessel and part thickness.

Disclosure statement

The authors report there are no competing interests to declare.

Funding

This work was supported by the EPSRC Future Composites Manufacturing Research Hub under Grant EP/P006701/1. Data collection was supported by Jason Mareo, Stuart Skyes, and Callum Heath at the National Composites Centre through a RCUK Catapult Researchers in Residence award EP/R513568/1.

Data availability

All underlying data to support the conclusions are provided within this paper.

References

1. Advani SG and Hsiao K-T. *Manufacturing techniques for polymer matrix composites (PMCs)*. Cambridge: Woodhead Publishing Limited, 2012.
2. Agius S, Magniez K and Fox B. Cure behaviour and void development within rapidly cured out-of-autoclave composites. *Composites Part B: Engineering* 2013; 47: 230-237.
3. Ghamlouch T. *Analysis of convective transfer around simple molds inside a model autoclave*. Doctoral dissertation, Université de Nantes, 2018.
4. Kluge N, Lundström T, Ljung A-L, Westerberg L-G, Nyman T and Composites. An experimental study of temperature distribution in an autoclave. *Journal of Reinforced Plastics* 2016; 35: 566-578.
5. Wang X, Zhang Z, Xie F, Li M, Dai D and Wang F. Correlated rules between complex structure of composite components and manufacturing defects in autoclave molding technology. *Journal of reinforced plastics and composites* 2009; 28: 2791-2803.
6. Slesinger N, Shimizu T, Arafath A and Poursartip A. Heat transfer coefficient distribution inside an autoclave. In: *17th international conference on composite material ICCM* Edinburgh, UK, 2009, IOM Communications.
7. Bohne T, Frerich T, Jendry J, Jürgens J-P and Ploshikhin V. Simulation and validation of air flow and heat transfer in an autoclave process for definition of thermal boundary conditions during curing of composite parts. *Journal of Composite Materials* 2018; 52: 1677-1687.
8. Kakac S, Yener Y and Pramuanjaroenkij A. *Convective heat transfer*. CRC press Boca Raton, 1995.
9. Zhu J, Frerich T and Herrmann AS. CFD modeling and validation of heat transfer inside an autoclave based on a mesh independency study. *Journal of Composite Materials* 2021; 55: 2469-2487.
10. Zobeiry N, Forghani A, Li C, Gordnian K, Thorpe R, Vaziri R, Fernlund G and Poursartip A. Multiscale characterization and representation of composite materials during processing. *Philosophical Transactions of the Royal Society A: Mathematical, Physical Engineering Sciences* 2016; 374: 20150278.
11. Weber TA, Arent J-C, Münch L, Duhovic M, Balvers JM and Manufacturing. A fast method for the generation of boundary conditions for thermal autoclave simulation. *Composites Part A: Applied Science* 2016; 88: 216-225.
12. Campbell Jr FC. *Manufacturing processes for advanced composites*. Oxford: elsevier, 2004.
13. Johnston AA. *An integrated model of the development of process-induced deformation in autoclave processing of composite structures*. Doctoral dissertation, University of British Columbia, 1997.
14. Dodiuk H. *Handbook of thermoset plastics*. Norwich, NY: William Andrew, 2022.

15. Hu H, Li S, Wang J, Zu L, Cao D and Zhong Y. Monitoring the gelation and effective chemical shrinkage of composite curing process with a novel FBG approach. *Composite structures* 2017; 176: 187-194.
16. Guo Q. *Thermosets: structure, properties, and applications*. Amsterdam: Woodhead Publishing, 2018.
17. Pusatcioglu S, Hassler J, Fricke A and McGee Jr H. Effect of temperature gradients on cure and stress gradients in thick thermoset castings. *Journal of Applied Polymer Science* 1980; 25: 381-393.
18. Yi S and Hilton HH. Effects of thermo-mechanical properties of composites on viscosity, temperature and degree of cure in thick thermosetting composite laminates during curing process. *Journal of Composite Materials* 1998; 32: 600-622.
19. Loos AC and Springer GS. Curing of epoxy matrix composites. *Journal of composite materials* 1983; 17: 135-169.
20. Ostrogorsky A. Simple explicit equations for transient heat conduction in finite solids. 2009.
21. Lienhard I and John H. *A Heat Transfer Textbook*. Cambridge, MA: Phlogiston Press, 2020.
22. Nam H, Lee K, Kim J, Chio S, Park J and Choi I. Experimental study on the emissivity of stainless steel. 2001.
23. Omega Engineering I. *The Infrared Temperature Handbook*. Omega Engineering, Incorporated, 1994.
24. Slesinger NA. *Thermal modeling validation techniques for thermoset polymer matrix composites*. University of British Columbia, 2010.
25. Mesogitis T, Kratz J and Skordos AA. Heat transfer simulation of the cure of thermoplastic particle interleaf carbon fibre epoxy prepregs. *Journal of Composite Materials* 2019; 53: 2053-2064.
26. Kamal M and Sourour S. Kinetics and thermal characterization of thermoset cure. *J Polymer Engineering Science* 1973; 13: 59-64.
27. Guo Z-S, Du S and Zhang B. Temperature field of thick thermoset composite laminates during cure process. *Composites science technology* 2005; 65: 517-523.
28. HexPly M21 Product Data Sheet. In: HEXCEL, (ed.). 2020.
29. Fourier JBJ and Darboux G. *Théorie analytique de la chaleur*. Didot Paris, 1822.
30. Lewis F. *Mechanical Engineering Handbook* Ed. Frank Kreith Boca Raton: CRC Press LLC, 1999. 1999.
31. Hilpert R. Heat transfer from cylinders. *Forsch Geb Ingenieurwes* 1933; 4: 215.
32. Raznjevic K. *Handbook of thermodynamic tables and charts*. Washington DC: Hemisphere Publication Corporation, 1976.
33. Kothandaraman C. *Fundamentals of heat and mass transfer*. 3rd ed. New Delhi: New Age International, 2006.
34. Dixon JC. *The shock absorber handbook*. 2nd ed. Chichester, England: John Wiley, 2007.
35. Ziegler F. The multiple meanings of the Stefan-number (and relatives) in refrigeration. *International journal of Refrigeration* 2010; 33: 1343-1349.
36. Invar - Nickel Iron Alloy, <https://www.azom.com/properties.aspx?ArticleID=515>.

Appendices

A1. Velocity field estimation

Numerous empirical correlations have been derived to capture the relationship between convective heat transfer (HTC) and fluid flow³⁰. These equations usually include Nusselt number (Nu), Reynolds number (Re) and Prandtl number (Pr). Nu quantifies the ratio of convective to conductive heat transfer in the fluid. It writes:

$$Nu = \frac{h_{con}l}{k_{gas}} \quad (A1)$$

where h_{con} is HTC, l is the characteristic length and k_{gas} is the thermal conductivity of the gas. Re is the ratio of inertial force to viscous forces in the fluid and is defined as

$$Re = \frac{\rho_{gas} v l}{\mu_{gas}} \quad (A2)$$

where v is the flow velocity, μ_{gas} and ρ_{gas} are the dynamic viscosity and density of the gas respectively. Pr is the ratio of momentum diffusivity to thermal diffusivity, written

$$Pr = \frac{C_p \mu_{gas}}{k_{gas}} \quad (A3)$$

The average velocity at each calorimeter during the temperature ramp to 180°C was computed using the Hilpert correlation for cylinders in cross flow³¹, defined as

$$Nu_D = C Re_D^n Pr^{\frac{1}{3}} \quad (A4)$$

where C and n depend on Re . The subscript D signifies that the characteristic length is the cylinder diameter. This correlation equation is applicable for $Pr \geq 0.7$ making it suitable for use with gases (Pr of air ~ 0.7 ³²). Flow inside autoclaves is generally turbulent³, given the orders of ρ_{gas} , μ_{gas} (Table A1) and the diameter (D) it was assumed Re was in the interval 4000-40000, which corresponded to C and n values of 0.193 and 0.618 respectively³³.

Equation (A4) was rearranged, and the dimensionless numbers expanded to obtain the velocity as,

$$v = \frac{\mu_{gas}}{\rho_{gas} D} \left[\frac{hD}{C} \left(\frac{1}{C_p \mu_{gas} k_{gas}^2} \right)^{\frac{1}{3}} \right]^{\frac{1}{n}} \quad (A5)$$

The properties of air were assumed constant during the ramp, the values used were obtained from standard properties and empirical relations³⁴ and are shown in Table A1.

A2. Approximate velocity fields

From Equation (A5) and Table A1 it can be seen that of the variables the velocity is dependent on, only HTC and density changed significantly between the tests. Equation (A5) also shows an inverse linear relationship between velocity and density, while velocity is proportional to HTC to the power of $1/n$, which is greater than unity. The effect of these variations is depicted in Figure A1, a box plot of the velocities in the vessels.

The low HTCs in the ovens translated into low velocities, again the uniquely high value observed in oven 5 is clearly visible. The velocity distribution changed significantly going to the autoclaves at 3 bars, with both the size of the values and variability increasing. This is due to the significant 176% increase in median HTC being sufficient to more than compensate for the accompanying increase in density. However, when the pressure is increased to 7 bars, the opposite is observed. The much smaller, 40% increase in median HTC is unable to compensate for the density which more than doubles, resulting in a plot that is closer to that of the ovens. Consequently, the approximations suggest that past a certain point, increasing

pressure results in a slower, less variable velocity field and hence diverges from the trend seen with the HTC measurements.

A3. Heat Transfer Sub-Model

The heat equation in the composite domain writes

$$\rho_c C_{p_c} \frac{dT}{dt} = \frac{d^2 k_c T}{dx^2} + L \frac{d\alpha}{dt} \quad (\text{A7})$$

where ρ_c is the effective density, C_{p_c} is the effective specific heat capacity, k_c is the effective through thickness thermal conductivity and L is the volumetric latent heat, defined as the product of the total heat of reaction, the density and volume fraction of the resin, taking values 415000Jkg^{-1} , 1280kgm^{-3} and 0.4 respectively²⁵.

In the laminate domain, effective density was the density of the fibres and resin joined through rule of mixtures assuming a fibre volume fraction of 0.6. The effective specific heat capacity and conductivity were functions of degree of cure and temperature. The effective specific heat capacity consisted of the values of the fibres $C_{p,f}$ and resin $C_{p,r}$ defined according to Equations (A8) and (A9) respectively, joined through rule of mixtures according to fibre weight fraction.

$$C_{p,f} = A_{f,c_p} T + B_{f,c_p} \quad (\text{A8})$$

$$C_{p,r} = A_{r,c_p} T + B_{r,c_p} + \frac{\Delta_{r,c_p}}{1 + \exp(C_{r,c_p}(T - T_g - s))} \quad (\text{A9})$$

where A_{r,c_p} and B_{r,c_p} , C_{r,c_p} , Δ_{r,c_p} and s are constants, the values of which were obtained by Mesogitis et al²⁵ from differential scanning calorimetry data. T_g is glass transition temperature. The effective transverse thermal conductivity of the laminate k was defined as follows,

$$k = A_k T + B_k \alpha + C_k T \alpha + D_k \quad (\text{A10})$$

where A_k , B_k , C_k and D_k are constants describing the linear dependence of conductivity on temperature, degree of cure, coupling effects and an offset, the values were derived by Mesogitis et al²⁵ using laser flash analysis.

The last term on the right-hand side of Equation (A7) was exclusive to the equation applied to the laminate, it represents the exothermic heat generated during the curing reaction and is responsible for the coupling between the cure kinetics and the heat transfer sub-models.

Convective heat transfer at the boundaries was defined by the Neumann boundary condition:

$$\frac{dkT}{dx} = -h(T - T_\infty) \quad (\text{A11})$$

A4. Cure Kinetics Sub-Model

The cure kinetics sub-model is representative of Hexply M21²⁸, a high-performance epoxy system with thermoplastic particle interleaf. Mesogitis et al²⁵ formulated the model for the

cure kinetics of this material based on a suitably modified variant of the Kamal and Sourour ²⁶ model,

$$\frac{d\alpha}{dt} = k_1(1 - \alpha)^{n_1} + k_2\alpha^m(1 - \alpha)^{n_2} \quad (\text{A12})$$

where α is degree of cure, n_1 , n_2 and m are reaction orders, and k_1 and k_2 are reaction constants. The reaction constants are composed of a diffusion term in addition to a chemical term to capture the effect of diffusion rate limitation phenomena post-vitrification, these terms are combined as

$$\frac{1}{k_i} = \frac{1}{k_{iC}} + \frac{1}{k_D} \quad i = 1,2 \quad (\text{A13})$$

where k_{iC} and k_D are the chemical and diffusion rate constants respectively. Both were assumed to have an Arrhenius temperature dependence

$$k_{iC} = A_i e^{\left(\frac{-E_i}{RT}\right)} \quad i = 1,2 \quad (\text{A14})$$

$$k_D = A_D e^{\left(\frac{-E_D}{RT}\right)} e^{\frac{-b}{f}} \quad (\text{A15})$$

where A_i and A_D are the pre-exponential factors, E_i and E_D are the activation energies, R is the universal gas constant, b is a constant and f is the equilibrium free volume, defined as

$$f = w(T - T_g) + g \quad (\text{A16})$$

where w is the thermal expansion coefficient of the free volume and g is the fractional free volume at T_g . T_g is degree of cure dependent according to the DiBenedetto equation

$$T_g = T_{g0} + \frac{\lambda\alpha(T_{g\infty} - T_{g0})}{1 - (1 - \lambda)\alpha} \quad (\text{A17})$$

where T_{g0} is the uncured glass transition temperature, $T_{g\infty}$ is the ultimate glass transition temperature and λ is a fitting parameter.

A5. Dimensional Analysis

To determine the contribution of the terms in the model to the rates of heat transfer and cure, and hence the need to include them, a dimensional analysis was performed. For simplicity, during this analysis C_{pc} and k_c were treated as constants with values for 90% DOC at 180°C. Although C_{pc} and k_c are cure and temperature dependent, the changes they undergo were sufficiently small (22% and 32% respectively) for meaningful qualitative deductions.

To nondimensionalise the heat equation four dimensionless variables were defined.

Dimensionless temperature T^* :

$$T^* = \frac{T(x, t) - T_0}{T_{dwell} - T_0} \quad (\text{A18})$$

where T_0 is initial temperature and T_{dwell} is the dwell temperature. Dimensionless time t^* was time divided by the duration of the initial ramp up t_{ramp} . The dimensionless thickness x^* was defined as x divided by the laminate domain thickness $|x_c|$. The ratio of the laminate domain

thickness $|x_c|$ to the tool domain thickness $|x_t|$ was denoted by the parameter A . The degree of cure α is already dimensionless.

First considering the nondimensionalisation of the heat equation in the laminate domain (Equation (A7)). After substitution of the dimensionless parameters and division by the coefficient of the temporal derivative, the coefficient of the spatial derivative took the form of the Fourier number Fo_c , written,

$$Fo_c = \frac{t_{ramp} k_c}{(\rho C_p)_c x_c^2} \quad (A19)$$

$$Fo_t = \frac{t_{ramp} k_t}{(\rho C_p)_t x_t^2} \quad (A20)$$

The coefficient of the rate of reaction term was the reciprocal of the Stephan number Ste or phase transition number Ph^{35} , defined as

$$Ph = Ste^{-1} = \frac{L}{(\rho C_p)_c (T_{dwell} - T_0)} \quad (A21)$$

Table 1. Descriptions of the curing vessels studied.

Vessel	Dimensions (m)	Temperature history	Pressure Profile	Airflow Description
Oven 1	0.50x0.58x0.75			Top and bottom inlets on right, to left wall, to right wall exhaust
Oven 2	0.62x1.24x0.62			Rear left inlet to central right wall exhaust
Oven 3	1.30x1.30x1.35	Ramp: 2°Cmin ⁻¹ Dwell: 155°C 10 min	Ambient	6 fans on rear wall, volume divided by 3 densely meshed shelves
Oven 4	20x5x5			From right wall inlets to left wall exhausts
Oven 5	5x5x5	Ramp 1: 5°Cmin ⁻¹ Dwell 1: 120°C 30 min Ramp 2: 1°Cmin ⁻¹ Dwell 2: 180°C 60 min		4 left inlets, 4 right inlets, to centre top exhaust
Autoclave 1	2x3			Bottom inlet to door to rear exhaust
Autoclave 2	2.6x4.5	Ramp: 2°Cmin ⁻¹ Dwell: 155°C 10 min	Ramp: 0.3bar/min Dwells: 3 & 7 bars	Top and bottom inlets to door to rear exhaust

Table 2. Parameters used in the coupled heat transfer and cure kinetics simulations^{25, 36}.

Parameter	Value
Effective laminate density	1580 kgm ⁻³
Fibre volume fraction	0.6
Volumetric latent heat	2.12e+8 Jm ⁻³
Tool density	8100 kgm ⁻³
Tool conductivity	15 Wm ⁻¹ K ⁻¹
Tool specific heat capacity	515 Jkg ⁻¹ K ⁻¹
Part thicknesses	5, 10, 15 mm
HTCs (temperature analysis)	25, 50, 150 Wm ⁻² K ⁻¹
HTCs (cure analysis)	15 - 215 Wm ⁻² K ⁻¹

Table 3. Cure time and temperature overshoot corresponding to the bounds of 95% confidence intervals for HTC in each vessel type assuming a normal distribution.

	Ovens	Autoclaves 3 bars	Autoclaves 7 bars
Cure time [min]	152.1, 154.8	170.7, 173.0	173.9, 175.2
Temperature Overshoot [°C]	14.5, 15.5	7.8, 9.1	6.4, 7.3

Table A1. The air properties at 180°C used during the velocity field approximations given in Equation (A5) (adapted from ³⁴).

Air property	P = 1 bar	P = 3 bars	P = 7 bars
Dynamic Viscosity (Nsm ⁻²)	2.504e-5	2.504e-5	2.504e-5
Density (kgm ⁻³)	0.769	2.307	5.383
Specific heat capacity (Jkg ⁻¹ K ⁻¹)	1019	1019	1019
Thermal conductivity (Wm ⁻¹ K ⁻¹)	0.036	0.036	0.036

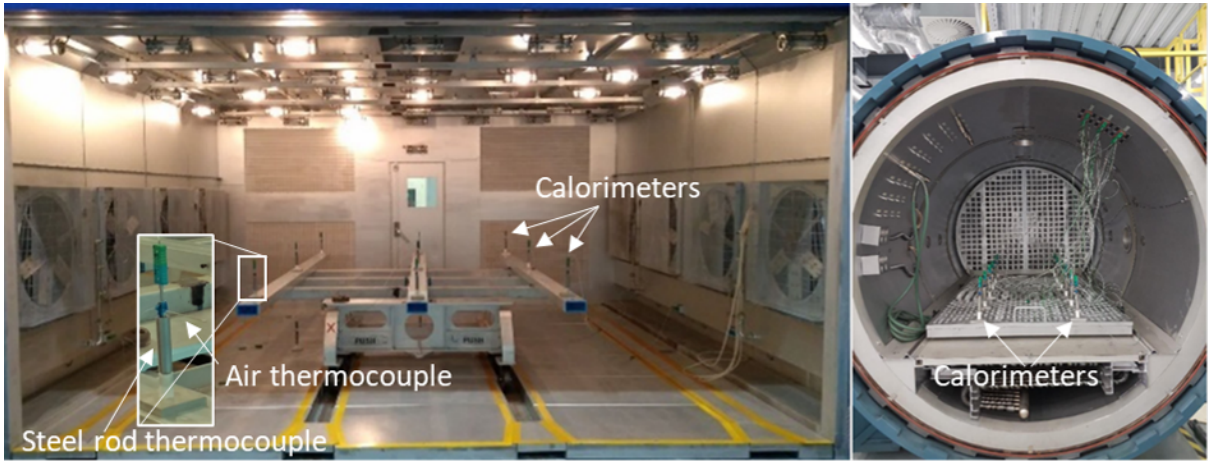


Figure 1. Images of two of the studied vessels, oven 5 (left) and autoclave 1 (right).

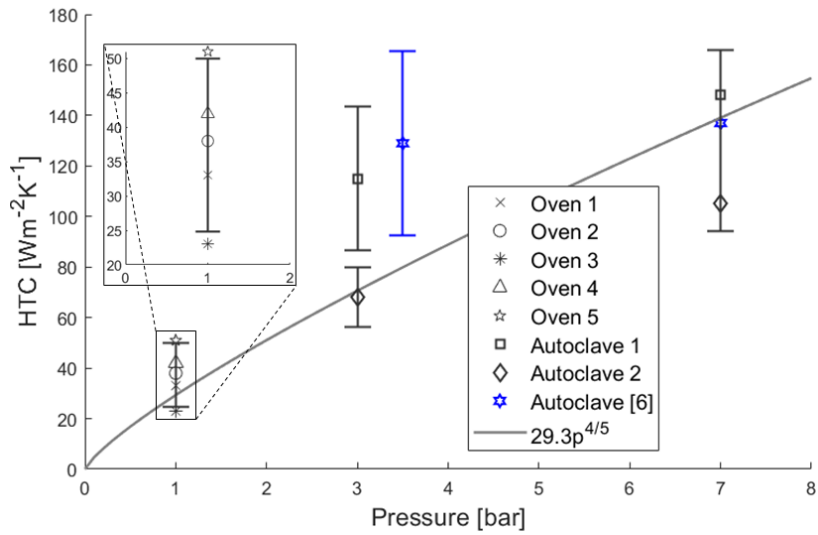


Figure 2. Spatial means of HTC measurements in each vessel during the two trials along with autoclave data from Slesinger [6]. Equation (8) model fit is also plotted. The error bars signify the standard deviations of the measurements. At 1 and 7 bars respectively, the error bar is the standard deviation of all the oven and autoclave data centred at the mean HTC.

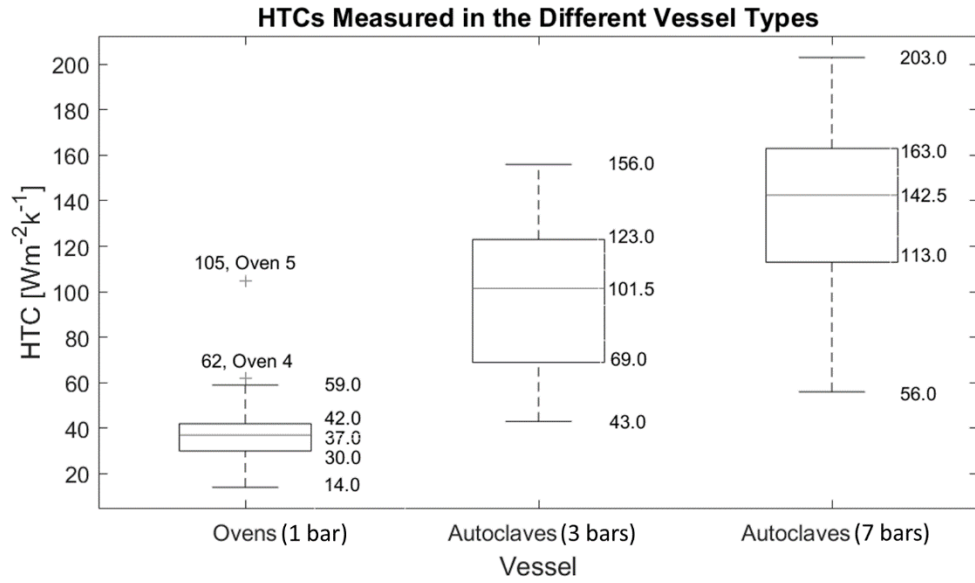


Figure 3. Measured HTC values in the ovens at 1 bar, and the autoclaves at 3 and 7 bars.

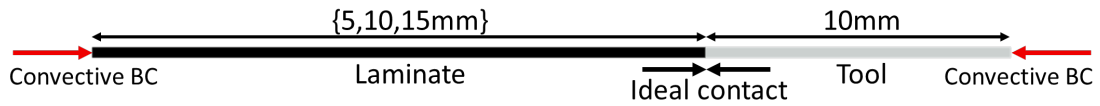


Figure 4. The geometry used in the FE model.

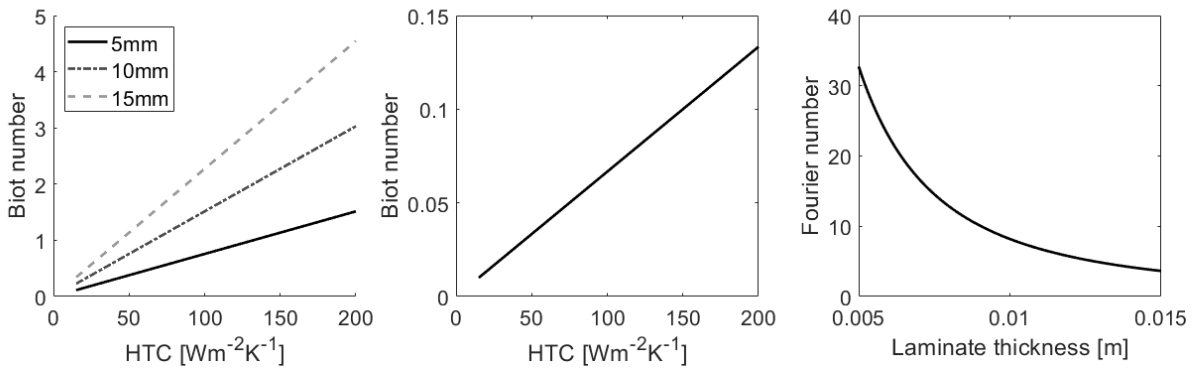


Figure 5. Variation of laminate (left) and tool (middle) Biot numbers with HTC, and laminate Fourier number with thickness (right). 90% DOC assumed where applicable.

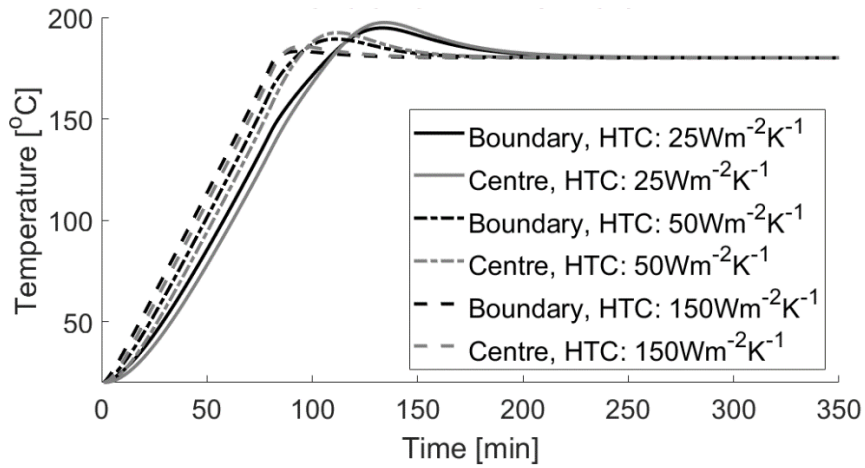


Figure 6. Air/laminate boundary and central laminate temperatures during the process. For HTCs of 25, 50 and 150Wm⁻²K⁻¹ with a 10mm thickness.

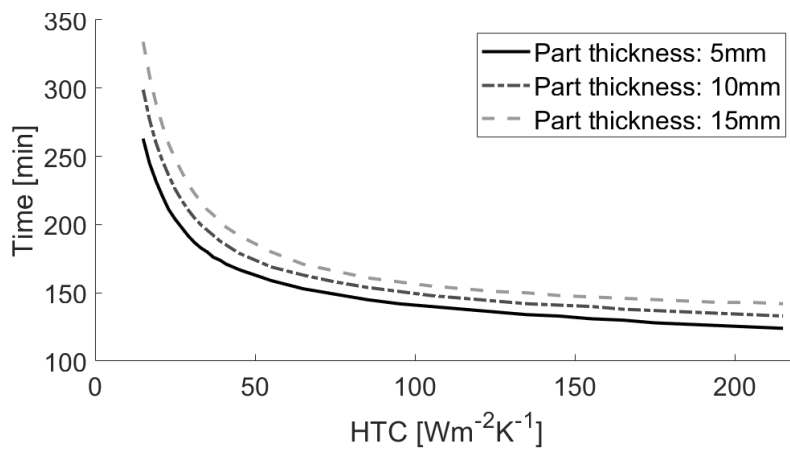


Figure 7. Time to reach dwell temperature over the range of observed HTCs for part thicknesses of 5, 10 and 15mm.

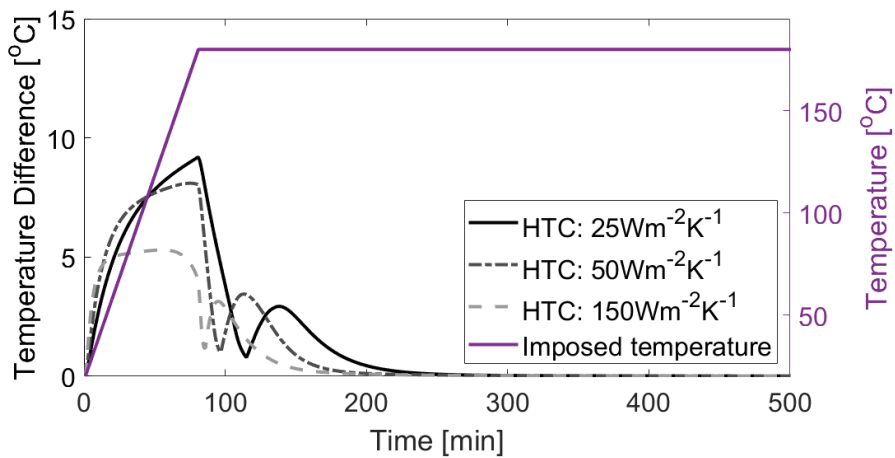


Figure 8. Maximum through thickness temperature difference with time for HTCs of 25, 50 and 150Wm⁻²K⁻¹ with a part thickness of 10mm.

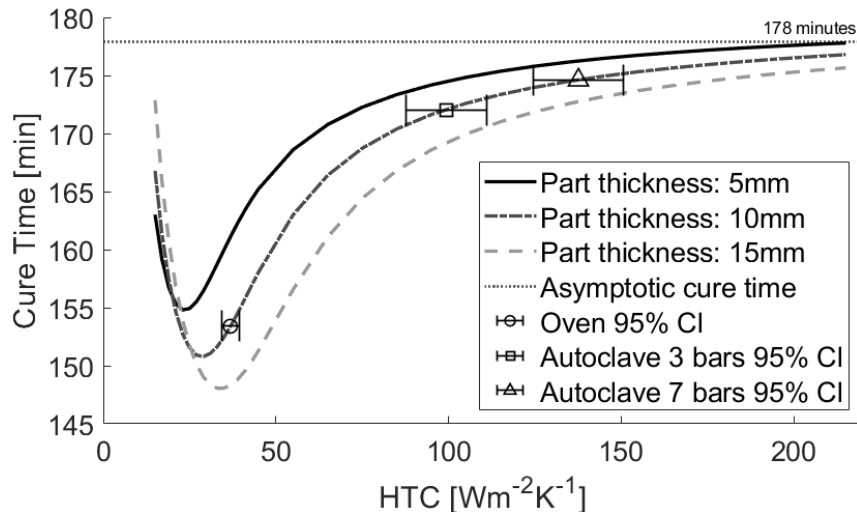


Figure 9. Cure time approximated for the geometry over the range of observed HTCs for part thicknesses of 5, 10 and 15mm. The cure time if the matter followed the cycle is 178 minutes. The error bars mark 95% confidence intervals (CI) for the specific case of HTC measured in the vessels.

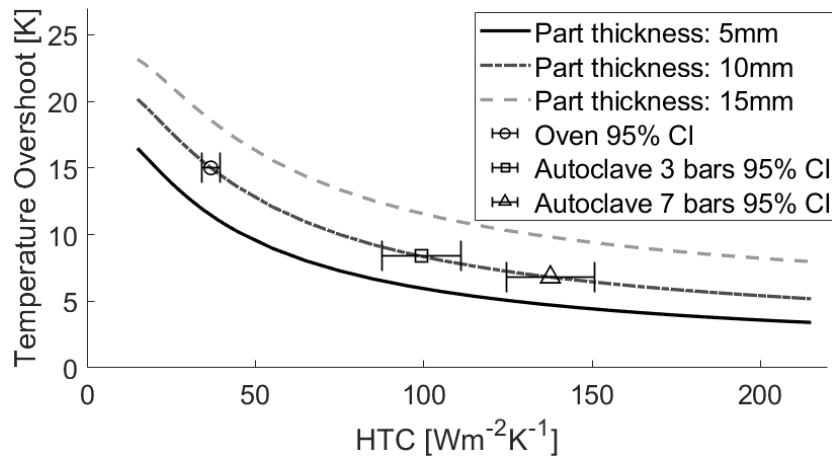


Figure 10. Temperature overshoot approximated for the geometry over the range of observed HTCs for part thicknesses of 5, 10 and 15mm. The error bars mark 95% confidence intervals (CI) for HTC measured in the vessels.

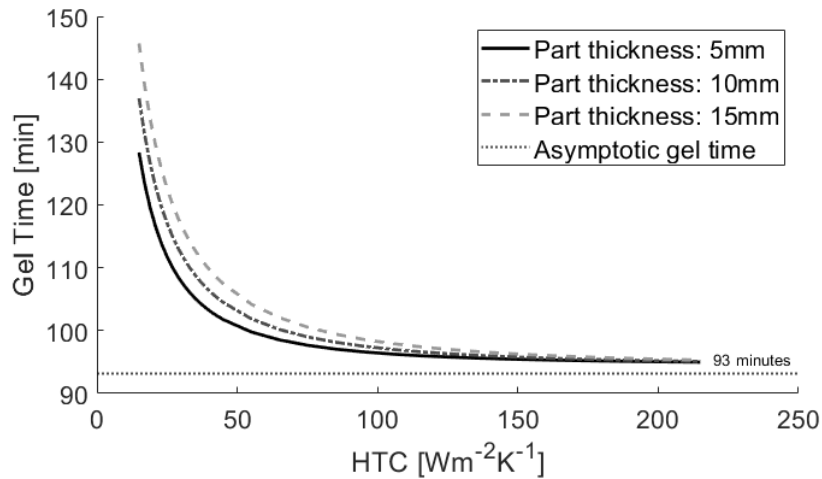


Figure 11. Gel time approximated for the geometry over the range of observed HTCs for part thicknesses of 5, 10 and 15mm. The gel time if the matter followed the cycle is 93 minutes.

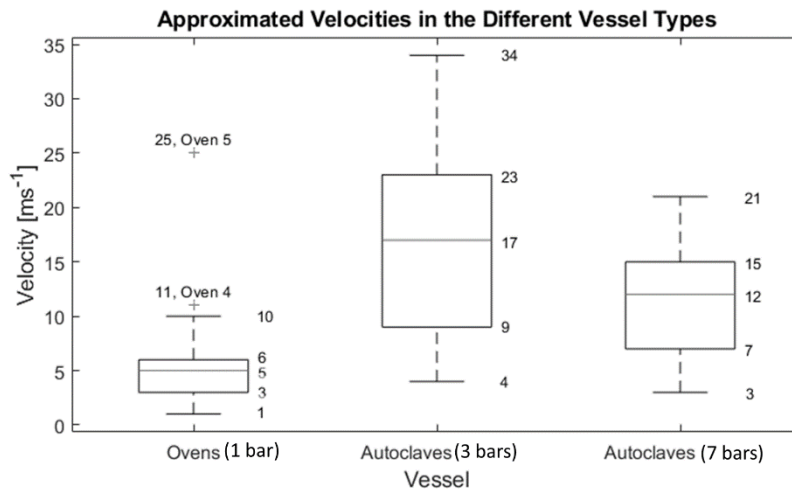


Figure A1. Approximated velocity values in the ovens, and the autoclaves at 3 and 7 bars.

Figure 1. Images of two of the studied vessels, oven 5 (left) and autoclave 1 (right).

Figure 2. Spatial means of HTC measurements in each vessel during the two trials along with autoclave data from Slesinger [6]. Equation (8) model fit is also plotted. The error bars signify the standard deviations of the measurements. At 1 and 7 bars respectively, the error bar is the standard deviation of all the oven and autoclave data centred at the mean HTC.

Figure 3. Measured HTC values in the ovens, and the autoclaves at 3 and 7 bars.

Figure 4. The geometry used in the FE model.

Figure 5. Variation of laminate (left) and tool (middle) Biot numbers with HTC, and laminate Fourier number with thickness (right). 90% DOC assumed where applicable.

Figure 6. Air/laminate boundary and central laminate temperatures during the process. For HTCs of 25, 50 and 150Wm⁻²K⁻¹ with a 10mm thickness.

Figure 7. Time to reach dwell temperature over the range of observed HTC's for part thicknesses of 5, 10 and 15mm.

Figure 8. Maximum through thickness temperature difference with time for HTC's of 25, 50 and $150\text{Wm}^{-2}\text{K}^{-1}$ with a part thickness of 10mm.

Figure 9. Cure time approximated for the geometry over the range of observed HTC's for part thicknesses of 5, 10 and 15mm. The cure time if the matter followed the cycle is 178 minutes. The error bars mark 95% confidence intervals (CI) for the specific case of HTC measured in the vessels.

Figure 10. Temperature overshoot approximated for the geometry over the range of observed HTC's for part thicknesses of 5, 10 and 15mm. The error bars mark 95% confidence intervals (CI) for HTC measured in the vessels.

Figure 11. Gel time approximated for the geometry over the range of observed HTC's for part thicknesses of 5, 10 and 15mm. The gel time if the matter followed the cycle is 93 minutes.

Figure A1. Approximated velocity values in the ovens, and the autoclaves at 3 and 7 bars.